HHS Public Access

Author manuscript

J Am Chem Soc. Author manuscript; available in PMC 2020 December 18.

Published in final edited form as:

J Am Chem Soc. 2020 February 12; 142(6): 2968–2974. doi:10.1021/jacs.9b11748.

In Situ Genetically Cascaded Amplification for Imaging RNA Subcellular Locations

Kewei Ren, **Rigumula Wu**, **Aruni P.K.K. Karunanayake Mudiyanselage**, **Qikun Yu**, **Bin Zhao**, **Yiwen Xie**, **Yousef Bagheri**, **Qian Tian**, **Mingxu You***

Department of Chemistry, University of Massachusetts, Amherst, Massachusetts 01003, USA

Abstract

In situ amplification methods, such as hybridization chain reaction, are valuable tools for mapping the spatial distribution and subcellular location of target analytes. However, the live-cell applications of these methods are still limited due to challenges in the probe delivery, degradation and cytotoxicity. Herein, we report a novel genetically encoded *in situ* amplification method to non-invasively image the subcellular location of RNA targets in living cells. In our system, a fluorogenic RNA reporter, Broccoli, was split into two non-fluorescent fragments and conjugated to the end of two RNA hairpin strands. The binding of one target RNA can then trigger a cascaded hybridization between these hairpin pairs and thus activate multiple Broccoli fluorescence signal. We have shown that such *in situ* amplified strategy can be used for the sensitive detection and location imaging of various RNA targets in living bacterial and mammalian cells. This new design principle provides an effective and versatile platform for tracking various intracellular analytes.

Graphical Abstract

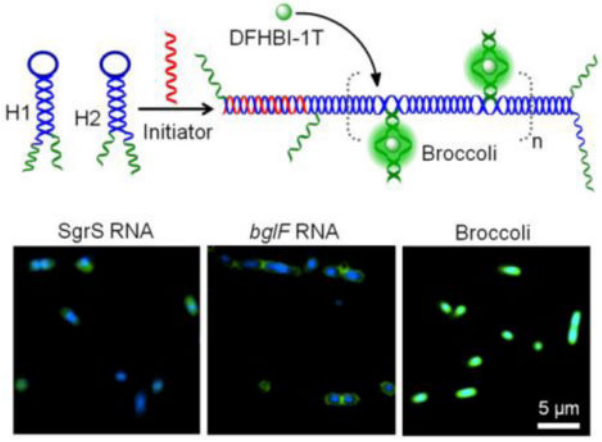

*Corresponding Author: mingxuyou@chem.umass.edu.

Supporting Information.

The Supporting Information is available free of charge via the Internet at http://pubs.acs.org.

Materials and Methods

Supplementary Tables 1 – 2

Supplementary Figures 1 – 12

INTRODUCTION

With high sensitivity and low detection limit, *in situ* amplification methods have emerged as a powerful technique for measuring the cellular concentration and subcellular location of target biomolecules.[1–4] For example, fluorescence *in situ* hybridization (FISH) is one of the gold standard techniques to reveal the cellular distributions of RNA and DNA molecules.[5–8] By conjugating with *in situ* amplification methods, such as hybridization chain reaction (HCR),[9–12] signal amplification by exchange reaction (SABER),[13,14] and click chemistry-based amplification (clampFISH),[15] the sensitivity and efficiency of FISH has been dramatically improved. However, these techniques require the delivery and multi-step washing of fluorophore-modified synthetic oligonucleotides. As a result, most of these methods are currently only applicable for fixed-cell imaging.[8,16,17]

In situ DNA-based amplification methods have also been used for live-cell imaging.[18–20] However, these synthetic DNA probes are still suffering from challenges including enzymatic degradations, difficulties in the probe delivery, and potential biosafety risks.[4] In contrast, we believe RNA-based amplification methods will be beneficial for live-cell applications. These RNA-based tools can be genetically encoded and directly transcribed inside living cells, which may be potentially useful for *in situ* signal amplification.

Fluorogenic RNA aptamers, such as Spinach or Broccoli, are specific RNA strands that can selectively bind and activate the fluorescence signal of nontoxic, cell-permeable small-molecule dyes.[21–23] Based on these fluorogenic RNAs, a series of biocompatible and genetically encoded sensors have been developed for non-invasive live-cell imaging of RNAs, proteins, small molecules, and metal ions.[24–32] However, without tagging multiple aptamers or achieving signal amplification, it remains a challenge for imaging low-abundance targets, especially in mammalian cells.[4,33,34]

In order to improve the sensitivity of fluorogenic RNA-based sensors, we have recently developed a signal amplification circuit based on RNA catalytic hairpin assembly, termed CHARGE, for low-abundance RNA imaging in living bacterial cells.[35] In this system, RNA target functioned as a catalyst and triggered the assembly of multiple RNA hairpins. However, after the reaction, target RNA was disconnected from the reporters. As a result, CHARGE cannot be used to track the subcellular location of the targets.

In this study, we developed an *IN SItu* Genetic Hybridization Amplification Technique, termed INSIGHT, for the sensitive imaging of the subcellular distributions and locations of RNA targets in living cells. Our approach is based on a combination of fluorogenic RNA reporters with RNA-based hybridization chain reaction (HCR). HCR is an enzyme-free and isothermal *in situ* amplification technique,[3,10] which has been applied for detection of a wide variety of analytes, including proteins, nucleic acids, and small molecules.[36–38]

In our INSIGHT design, in the absence of initiator RNAs, two types of RNA hairpins (H1 and H2) coexisted under a metastable state (Figure 1). Upon the addition of an initiator RNA, the H1 hairpin will be opened and expose a sequence that can invade and hybridize with the H2 hairpin. A cascaded hybridization between these two hairpins was then initiated and generated a double-stranded concatemeric nanostructure.

We have further split RNA Broccoli into two non-fluorescent fragments and separately conjugated them to each end of the H1 and H2 hairpins (Figure S1). These two fragments cannot be spontaneously hybridized to activate Broccoli fluorescence (Figure S2).[24] In the presence of an initiator RNA, the cascaded H1/H2 hybridization induced the reassembly of a chain of Broccoli and thus activated an amplified fluorescence signal (Figure 1). Importantly, the generated chain of Broccoli will be associated with the initiator strand, which can be used for the cellular tracking. Herein, we demonstrated that such an *in situ* amplification method can be genetically encoded and used for the detection and location imaging of various RNA targets in both bacterial and mammalian cells.

RESULTS

Design and Optimization of the INSIGHT System.

We first asked how we can split the Broccoli RNA to display weak fluorescence signal when separately labeled at the 5'- and 3'- end of the hairpin, and meanwhile, upon the initiator-triggered H1/H2 hybridization, reassemble and activate the fluorescence of a small-molecule dye, 3,5-difluoro-4-hydroxybenzylidene-1-trifluoroethyl-imidazolinone (DFHBI-1T) (Figure 1).

We started by testing a design of Broccoli splits similar as that was used in our recent development of CHARGE (Figure S1a). Two Broccoli fragments were then conjugated to each end of an H1/H2 hairpin pair. This hairpin pair has been previously used in developing HCR.[39] After we *in vitro* synthesized these RNA strands (termed D1), however, a high background signal was observed, even in the solution containing only H1 or H2 (Figure S1b). We realized that such background signal was likely due to the spontaneous assembly of Broccoli within each hairpin. To reduce this background, we decided to decrease the number of base pairs between two Broccoli fragments (D2). Indeed, the background was dramatically reduced in D2 but limited signal enhancement was observed after adding the initiator (Figure 2a and S1c).

To increase the signal-to-background (S/B) ratio, we came up with a new sensor design principle by blocking two (D3) or four (D4) nucleotides of Broccoli within the stem region of H1 and H2 hairpins (Figure S1d and S1e). In the absence of initiator, these blocked nucleotides were not able to spontaneously assemble into Broccoli, i.e., a low background signal. While upon the addition of initiator RNA, the cascaded assembly of H1 and H2 triggered the release of these blocked nucleotides and exhibited high fluorescence activation. Indeed, compared with D1 (1.5-fold) and D2 (1.2-fold), an increased fluorescence enhancement was observed for D3 (1.8-fold) and D4 (2.1-fold) (Figure 2a).

We realized that even though the background fluorescence has been effectively reduced in solution containing either H1 or H2, after mixing these two hairpin strands, an obvious increase in the fluorescence signal was shown (Figure S1). One potential reason for such undesired signal should be the spontaneous unfolding of H1 or H2 hairpin. To further improve the stability of both hairpins, we tried to increase the stem lengths of H1 and H2. Indeed, an optimal design of RNA hairpin pairs (D5) was achieved in this way, with low

background and large signal enhancement (3.0-fold) in the presence of initiator (Figure 2a). D5 was thus selected to conduct the subsequent experiments.

In Vitro RNA Detection with INSIGHT.

After optimizing the sequences of INSIGHT, we next tested the performance of this *in situ* amplification approach under different environmental conditions. We first studied the effect of different buffers on the fluorescence signal, including HEPES, Tris-buffered saline, and phosphate-buffered saline (Figure S3a). INSIGHT can be used for initiator RNA detection in all these buffers. The largest S/B ratio was observed in the HEPES buffer, which was used in the subsequent *in vitro* tests. Magnesium ion (Mg^{2+}) concentration is another important parameter affecting RNA folding and the efficiency of hybridization chain reactions. An enhanced INSIGHT signal was observed after increasing Mg^{2+} concentration in the range of 1–10 mM (Figure S3b). However, the background signal was also enhanced at the same time. A similar S/B ratio was observed in the presence of 1 mM (2.2-fold), 5 mM (2.3-fold), or 10 mM (2.3-fold) Mg^{2+} ions (Figure S3b), indicating that INSIGHT can function well in the presence of physiological concentrations of Mg^{2+} ions (~1–2 mM).[40,41]

We have further studied the effect of temperature and incubation time on the INSIGHT system. At both 22°C and 37°C, the initiator-induced INSIGHT signal gradually increased over the 5 h incubation time, with 90% of maximum fluorescence observed after ~2.5 h incubation (Figure S3c and S3d). The optimal S/B ratio was achieved after 4 h incubation at 22°C (3.1-fold) or 3 h incubation at 37°C (2.9-fold). These results together indicated that INSIGHT can be used for detection of initiator RNA under different conditions.

We next asked if INSIGHT can be used for detecting low-abundance initiator RNA. As shown in Figure 2b, after incubating various concentrations of initiator, 2–250 nM, with 250 nM H1/H2 (D5) and 5.0 μM DFHBI-1T, a dose-response curve was generated. A clear initiator-induced fluorescence activation was observed, with a detection limit of 1.9 nM. As a control, under the same condition, the minimal detectable amount of Broccoli was 30.2 nM (Figure S4), a 15-fold difference from that of INSIGHT. We have further used a native gel electrophoresis assay to characterize the product of hybridization chain reactions (Figure S4). Indeed, long RNA product bands could be visualized only in the presence of initiator RNA, even when the initiator concentration was 50-fold lower than that of the hairpins (Figure S5). Indeed, INSIGHT can be used to detect low-abundance RNAs.

RNA Imaging in Bacterial Cells with INSIGHT.

We next applied INSIGHT for RNA imaging in live *E. coli* cells. We first cloned the H1 and H2 sequences into a dual-expression pETDuet vector, and the initiator sequence in a pCDFDuet vector. After transformation and isopropyl β–D−1-thiogalactopyranoside (IPTG) induction, an intense cellular fluorescence signal was observed (Figure 3). This signal was comparable with that of Broccoli-expressing cells. As a control, cells that were transformed with only H1 or H2, or the mixture of H1 and H2 (H1/H2), displayed minimal fluorescence intensity (Figure 3). We have further determined the cellular fluorescence levels from 300 individual *E. coli* cells in each case. On average, compared with cells expressing H1/H2, a

3.0-fold signal enhancement was observed in the presence of initiator RNA (H1/H2/I). Indeed, INSIGHT can be activated for the cellular imaging of RNAs.

We also wanted to study the kinetics of INSIGHT in living cells. After IPTG induction, we imaged the cells expressing H1/H2 or H1/H2/I every one hour during a total of 4 h incubation (Figure S6). In the presence of initiator RNA, INSIGHT signal can be visualized after only 1 h incubation, while the maximum cellular fluorescence was shown in 3 h. Minimal H1/H2 fluorescence was observed in the same period. While longer incubation time will indeed enhance the background signal of the spontaneous hybridization between H1 and H2 (Figure S6). As a result, ~3 h incubation was optimal with enhanced S/B ratio.

We next asked if we can develop a modular INSIGHT system to image different RNA sequences of interest. For this purpose, an RNA molecular beacon was introduced into the system (Figure 4a). The loop sequence of the molecular beacon can be changed to hybridize with different RNA targets. These molecular beacons also contained a conserved stem region. Part of the initiator strand was blocked in this stem. Target binding induced the dehybridization of the stem, activated the initiator RNA, which further induced a cascaded hybridization between H1 and H2. As a result, the same sequence of H1 and H2 can be used to detect various RNA targets.

To test this idea, we first designed a molecular beacon to detect SgrS, a small RNA involved in bacterial glucose transportation.[42] Three molecular beacons containing 7, 8, or 10 base pairs in the stem region were *in vitro* synthesized, and then the corresponding INSIGHT signal was measured in the presence or absence of 20 nM SgrS (Figure 4b). Based on the large S/B ratio, an optimal molecular beacon structure with a 7-base-pair stem (7B) was identified for further studies.

We next asked if we can image SgrS RNA in living *E. coli* cells. The 7B molecular beacon was cloned into a pCDFDuet vector and then co-transformed with the pETDuet-H1/H2 vector into BL21 (DE3)* cells. It is known that the cellular expression of SgrS can be induced by adding glucose.[43] Indeed, in the presence of 0–20 g/L glucose, an enhanced cellular fluorescence was observed with the increasing amount of glucose (Figure 4c). As a control, after adding the same concentration of glucose, there is almost no change in the fluorescence signal from cells expressing Broccoli or H1/H2/I (Figure S7).

We have further used real-time PCR to quantify the cellular level of SgrS RNA after adding glucose. Consistent with some previous studies,[44] our results indicated that 24–70 nM concentration of SgrS was generated in the presence of 0–20 g/L glucose (Figure S8). Based on the corresponding cellular fluorescence (Figure 4), INSIGHT can be used for the sensitive imaging of low-abundance (~30 nM) target RNA in living cells.

INSIGHT-based Imaging of the Subcellular Location of Target RNAs.

Our next goal is to study if we can use INSIGHT to study the subcellular distribution of target RNAs. We chose SgrS and a *bglF* mRNA as the targets, since the cellular location of both of these two RNAs have been well characterized.[44,45] By simply changing the loop

region of the molecular beacon, an INSIGHT system was developed to detect *bglF* RNA using the same H1/H2 hairpins (Figure S9).

After expressing the SgrS- or *bglF*-targeting INSIGHT system in BL21 (DE3)* cell, a 4',6-diamidino-2-phenylindole (DAPI) dye was also added to stain the location of the nucleoid. Consistent with previously reported FISH-based images,[44,45] the SgrS RNA predominantly located in the cytoplasm (71.1%) in *E. coli* cells, whereas the transcripts encoding *bglF* were detected mainly (82.5%) nearby the cell membranes (Figure 5). Both fluorescence signals exhibited little overlap with that of DAPI (Figure S10). As another control, the fluorescence signal of similarly transcribed Broccoli was homogeneously distributed throughout the whole cell region (Figure 5 and S10). All these results suggested that INSIGHT can indeed be used to study the spatial distribution and subcellular location of target RNAs.

RNA Imaging in Mammalian Cells with INSIGHT.

After demonstrating the performance of INSIGHT in bacterial cells, we next asked if this system can also be used for RNA imaging in mammalian cells. We first cloned the H1, H2 and initiator sequences into an AIO-Puro vector (H1/H2/I), which contains three U6 promoter regions. After transfecting this vector into HeLa cells, obvious cellular fluorescence can be visualized (Figure S11). On average, cells expressing H1/H2/I (activated INSIGHT) exhibited 2.4-fold higher fluorescence signal than those expressing H1/H2, and 2.2-fold brighter than those expressed H1/H2/random sequence (Figure S11). Indeed, INSIGHT can be potentially used for RNA imaging in mammalian cells.

We then applied INSIGHT for imaging endogenous mRNAs in mammalian cells. We first developed a molecular beacon probe (termed SMB) to target *survivin* mRNA (Table S2). The resultant *survivin*-targeting INSIGHT exhibited a similar level of fluorescence enhancement as that induced by the initiator strand (Figure 6a). In contrast, when using a control molecular beacon of random loop sequence (C-SMB), little fluorescence enhancement was observed after adding *survivin* RNA.

We next cloned SMB, together with H1 and H2, into the above-mentioned AIO-Puro vector. After transfecting into HeLa cells, fluorescence activations could be clearly observed in the cytoplasm (Figure 6b and S12). This result is consistent with some previous studies in HeLa cells for the subcellular location of *survivin* mRNA.[46,47] As a control, negligible fluorescence signal was observed in cells expressing H1/H2 or H1/H2/C-SMB. To further confirm that the observed fluorescence signals indeed indicated the cellular expression of *survivin* mRNA, we treated the cells with YM155, a survivin inhibitor that is known to suppress the expression of *survivin* mRNA in HeLa cells.[48] As expected, after adding YM155, the cellular fluorescence signals disappeared even in cells expressing H1/H2/SMB (Figure 6b, 6c, and S12). Indeed, these results indicated that INSIGHT can be used for target mRNA imaging in mammalian cells.

DISCUSSION

DNA-based *in situ* amplification methods have been used to visualize and quantify the subcellular distributions of nucleic acids, proteins and small molecules. However, the live-

cell applications of these methods are still limited, mainly due to the challenges in the probe delivery and degradation. Here, we report a novel genetically encoded RNA-based *in situ* amplification approach, termed INSIGHT. By conjugating fluorogenic RNA aptamers with hybridization chain reactions, INSIGHT can be used to image target RNAs in living bacterial and mammalian cells.

The INSIGHT system has several important features for cellular imaging. (1) The INSIGHT probes can be genetically encoded and directly transcribed inside cells, obviating the invasive delivery process. (2) Target-triggered hybridization chain reaction amplifies the signal and improves the sensitivity of the approach, which is especially important for low-abundance target imaging. (3) As an *in situ* amplification method, INSIGHT can be used for imaging the spatiotemporal distributions of target analytes. In addition, the fluorescence signals were concentrated in several localized spots, and as a result, it can be brighter and easier to observe than those signals dispersed in the homogeneous solution. (4) By simply changing the loop region of a molecular beacon, the INSIGHT system can be conveniently designed to detect different target RNAs. As a result, INSIGHT is a modular and universal platform for the cellular imaging of various target analytes.

The concatemeric nanostructure generated by INSIGHT activation may also potentially improve the intracellular folding and/or enzymatic resistance of fluorogenic RNAs. By replacing Broccoli with other fluorogenic RNA aptamers such as DNB,[49] Corn,[50,51] Mango,[52] and Pepper,[34] it should be possible to extend the potential applications of INSIGHT for the multi-color imaging of cellular analytes.

In addition to their applications in the cellular imaging, these genetically encoded hybridization chain reactions may be potentially used to build up intracellular RNA scaffolds for the programmable regulation of cellular functions.[53] Indeed, synthetic RNA scaffolds have been applied to spatially organize multi-enzyme complexes.[54,55] By changing Broccoli into protein-binding aptamers, INSIGHT can be potentially used to build target-responsive artificial cellular network.

In sum, we envision this INSIGHT system can be broadly applied for sensing intracellular molecules of interest. INSIGHT can be used for real-time imaging of the subcellular locations and interactions of target analytes. The rational design of INSIGHT can also be potentially useful in regulating metabolic pathways and cellular functions.

Supplementary Material

Refer to Web version on PubMed Central for supplementary material.

ACKNOWLEDGMENT

The authors gratefully acknowledge the UMass Amherst start-up grant, NIH R01AI136789, NSF CAREER, and Alfred P. Sloan Research Fellowship to M. You. Q. Yu is also supported by NIH T32GM008515. We are grateful to Dr. James Chambers for the assistance in the fluorescence imaging. The authors also thank other members in the You Lab and Dr. Craig Martin for useful discussion and valuable comments.

REFERENCES

1. Deng R; Zhang K; Wang L; Ren X; Sun Y; Li J DNA-Sequence-Encoded Rolling Circle Amplicon for Single-Cell RNA Imaging. Chem 2018, 4 (6), 1373–1386.
2. Simmel FC; Yurke B; Singh HR Principles and Applications of Nucleic Acid Strand Displacement Reactions. Chem. Rev 2019, 119 (10), 6326–6369. [PubMed: 30714375]
3. Bi S; Yue S; Zhang S Hybridization Chain Reaction: A Versatile MolecularTool for Biosensing, Bioimaging, and Biomedicine. Chem. Soc. Rev 2017, 46 (14), 4281–4298. [PubMed: 28573275]
4. Qing Z; Xu J; Hu J; Zheng J; He L; Zou Z; Yang S; Tan W; Yang R In Situ Amplification-Based Imaging of RNA in Living Cells. Angew. Chem. Int. Ed 2019, 58 (34), 11574–11585.
5. Vargas DY; Shah K; Batish M; Levandoski M; Sinha S; Marras SA; Schedl P; Tyagi S Single-molecule Imaging of Transcriptionally Coupled and Uncoupled Splicing. Cell 2011, 147 (5), 1054–1065. [PubMed: 22118462]
6. Deng W; Shi X; Tjian R; Lionnet T; Singer RH CASFISH: CRISPR/Cas9-mediated in Situ Labeling of Genomic Loci in Fixed Cells. Proc. Natl. Acad. Sci. U S A 2015, 112 (38), 11870–11875. [PubMed: 26324940]
7. Beliveau BJ; Boettiger AN; Avendano MS; Jungmann R; McCole RB; Joyce EF; Kim-Kiselak C; Bantignies F; Fonseka CY; Erceg J; Hannan MA; Hoang HG; Colognori D; Lee JT; Shih WM; Yin P; Zhuang X; Wu CT Single-molecule Super-resolution Imaging of Chromosomes and in Situ Haplotype Vsualization Using Oligopaint FISH Probes. Nat. Commun 2015, 6, 7147. [PubMed: 25962338]
8. Levsky JM; Singer RH Fluorescence in Situ Hybridization: Past, Present and Future. J. Cell. Sci 2003, 116 (14), 2833–2838. [PubMed: 12808017]
9. Dirks RM; Pierce NA Triggered Amplification by Hybridization Chain Reaction. Proc. Natl. Acad. Sci. U.S.A 2004, 101 (43), 15275–15278. [PubMed: 15492210]
10. Evanko D Hybridization Chain Reaction. Nat. Methods 2004, 1, 186.
11. Choi HMT; Schwarzkopf M; Fornace ME; Acharya A; Artavanis G; Stegmaier J; Cunha A; Pierce NA Third-generation in Situ Hybridization Chain Reaction: Multiplexed, Quantitative, Sensitive, Versatile, Robust. Development 2018, 145 (12), 1–10.
12. Choi HMT; Beck VA; Pierce NA Next-Generation in Situ Hybridization Chain Reaction: Higher Gain, Lower Cost, Greater Durability. ACS Nano 2014, 5, 4284–4294.
13. Kishi JY; Lapan SW; Beliveau BJ; West ER; Zhu A; Sasaki HM; Saka SK; Wang Y; Cepko CL; Yin P SABER Amplifies FISH: Enhanced Multiplexed Imaging of RNA and DNA in Cells and Tissues. Nat. Methods 2019, 16 (6), 533–544. [PubMed: 31110282]
14. Saka SK; Wang Y; Kishi JY; Zhu A; Zeng Y; Xie W; Kirli K; Yapp C; Cicconet M; Beliveau BJ; Lapan SW; Yin S; Lin M; Boyden ES; Kaeser PS; Pihan G; Church GM; Yin P Immuno-SABER Enables Highly Multiplexed and Amplified Protein Imaging in Tissues. Nat. Biotechnol 2019, 37 (9), 1080–1090. [PubMed: 31427819]
15. Rouhanifard SH; Mellis IA; Dunagin M; Bayatpour S; Jiang CL; Dardani I; Symmons O; Emert B; Torre E; Cote A; Sullivan A; Stamatoyannopoulos JA; Raj A ClampFISH Detects Individual Nucleic Acid Molecules Using Click Chemistry-based Amplification. Nat. Biotechnol 2018, 37, 84–89.
16. Buxbaum AR; Haimovich G; Singer RH In the Right Place at the Right Time: Visualizing and Understanding mRNA Localization. Nat. Rev. Mol. Cell Biol 2015, 16 (2), 95–109. [PubMed: 25549890]
17. Kannaiah S; Amster-Choder O Methods for Studying RNA Localization in Bacteria. Methods 2016, 98, 99–103. [PubMed: 26707207]
18. Chu H; Zhao J; Mi Y; Zhao Y; Li L Near-Infrared Light-Initiated Hybridization Chain Reaction for Spatially and Temporally Resolved Signal Amplification. Angew. Chem. Int. Ed 2019, (58), 1–7.
19. Wu Z; Liu GQ; Yang XL; Jiang JH Electrostatic Nucleic Acid Nanoassembly Enables Hybridization Chain Reaction in Living Cells for Ultrasensitive mRNA Imaging. J. Am. Chem. Soc 2015, 137 (21), 6829–6836. [PubMed: 25969953]

20. Wu C; Cansiz S; Zhang L; Teng IT; Qiu L; Li J; Liu Y; Zhou C; Hu R; Zhang T; Cui C; Cui L; Tan W A Nonenzymatic Hairpin DNA Cascade Reaction Provides High Signal Gain of mRNA Imaging inside Live Cells. J. Am. Chem. Soc 2015, 137 (15), 4900–4903. [PubMed: 25835750]
21. Neubacher S; Hennig S RNA Structure and Cellular Applications of Fluorescent Light-Up Aptamers. Angew. Chem. Int. Ed 2019, 58 (5), 1266–1279.
22. You M; Jaffrey SR Structure and Mechanism of RNA Mimics of Green Fluorescent Protein. Annu. Rev. Biophys 2015, 44, 187–206. [PubMed: 26098513]
23. Sun Z; Nguyen T; McAuliffe K; You M Intracellular Imaging with Genetically Encoded RNA-based Molecular Sensors. Nanomaterials 2019, 9 (2), 233.
24. Wang Z; Luo Y; Xie X; Hu X; Song H; Zhao Y; Shi J; Wang L; Glinsky G; Chen N; Lal R; Fan C In Situ Spatial Complementation of Aptamer-Mediated Recognition Enables Live-Cell Imaging of Native RNA Transcripts in Real Time. Angew. Chem. Int. Ed 2018, 57 (4), 972–976.
25. Ying ZM; Wu Z; Tu B; Tan W; Jiang JH Genetically Encoded Fluorescent RNA Sensor for Ratiometric Imaging of MicroRNA in Living Tumor Cells. J. Am. Chem. Soc 2017, 139 (29), 9779–9782. [PubMed: 28714696]
26. Song W; Strack RL; Jaffrey SR Imaging Bacterial Protein Expression Using Genetically Encoded RNA Sensors. Nat. Methods 2013, 10 (9), 873–875. [PubMed: 23872791]
27. You M; Litke JL; Jaffrey SR Imaging Metabolite Dynamics in Living Cells Using a Spinach-based Riboswitch. Proc. Natl. Acad. Sci. U. S. A 2015, 112 (21), E2756–2765. [PubMed: 25964329]
28. Paige JS; Nguyen-Duc T; Song W; Jaffrey SR Fluorescence Imaging of Cellular Metabolites with RNA. Science 2012, 335 (6073), 1194. [PubMed: 22403384]
29. Yu Q; Shi J; Mudiyanselage A; Wu R; Zhao B; Zhou M; You M Genetically Encoded RNA-based Sensors for Intracellular Imaging of Silver Ions. Chem. Commun 2019, 55 (5), 707–710.
30. Su Y; Hickey SF; Keyser SG; Hammond MC In Vitro and In Vivo Enzyme Activity Screening via RNA-Based Fluorescent Biosensors for S-Adenosyl-l-homocysteine (SAH). J. Am. Chem. Soc 2016, 138 (22), 7040–7047. [PubMed: 27191512]
31. Wang XC; Wilson SC; Hammond MC Next-generation RNA-based Fluorescent Biosensors Enable Anaerobic Detection of Cyclic di-GMP. Nucleic. Acids Res 2016, 44 (17), e139. [PubMed: 27382070]
32. Wu R; Karunanayake Mudiyanselage A; Shafiei F; Zhao B; Bagheri Y; Yu Q; McAuliffe K; Ren K; You M Genetically Encoded Ratiometric RNA-Based Sensors for Quantitative Imaging of Small Molecules in Living Cells. Angew. Chem. Int. Ed 2019, 58, 18271–18275.
33. Karunanayake Mudiyanselage A; Wu R; Leon-Duque MA; Ren K; You M “Second-generation” Fluorogenic RNA-based Sensors. Methods 2019, 161, 24–34. [PubMed: 30660865]
34. Chen X; Zhang D; Su N; Bao B; Xie X; Zuo F; Yang L; Wang H; Jiang L; Lin Q; Fang M; Li N; Hua X; Chen Z; Bao C; Xu J; Du W; Zhang L; Zhao Y; Zhu L; Loscalzo J; Yang Y Visualizing RNA Dynamics in Live Cells with Bright and Stable Fluorescent RNAs. Nat. Biotechnol 2019, 36, 1136–1148.
35. Karunanayake Mudiyanselage A; Yu Q; Leon-Duque MA; Zhao B; Wu R; You M Genetically Encoded Catalytic Hairpin Assembly for Sensitive RNA Imaging in Live Cells. J. Am. Chem. Soc 2018, 140 (28), 8739–8745. [PubMed: 29944357]
36. Augspurger EE; Rana M; Yigit MV Chemical and Biological Sensing Using Hybridization Chain Reaction. ACS. Sens 2018, 3 (5), 878–902. [PubMed: 29733201]
37. Yang DW; Tang YG; Miao P Hybridization Chain Reaction Directed DNA Superstructures Assembly for Biosensing Applications. TRAC-Trend Anal. Chem 2017, 94, 1–13.
38. Park CR; Park SJ; Lee WG; Hwang BH Biosensors Using Hybridization Chain Reaction - Design and Signal Amplification Strategies of Hybridization Chain Reaction. Biotechnol. Bioprce 2018, 23 (4), 355–370.
39. Choi HM; Chang JY; Trinh le A; Padilla JE; Fraser SE; Pierce NA Programmable in Situ Amplification for Multiplexed Imaging of mRNA Expression. Nat. Biotechnol 2010, 28 (11), 1208–1212. [PubMed: 21037591]
40. G. RDIntracellular Magnesium and Magnesium Buffering. BioMetals 2002, 15, 251–259. [PubMed: 12206391]

41. Alatossava T J. H; Kuhn A; Kellenberger E. Manipulation of Intracellular Magnesium Content in Polymyxin B Nonapeptide-Sensitized Escherichia coli by lonophore A23187. J. Bacteriol 1985 162(1), 413–419. [PubMed: 2984182]

42. Bobrovskyy M; Vanderpool CK The Small RNA SgrS: Roles in Metabolism and Pathogenesis of Enteric Bacteria. Front. Cell. Infect. Microbiol 2014, 4 (61), 1–9. [PubMed: 24478989]

43. Negrete A; Ng WI; Ng WI Glucose Uptake Regulation in E. coli by the Small RNA SgrS: Comparative Analysis of E. coli K-12 (JM109 and MG1655) and E. coli B (BL21). Microb. Cell Fact 2010, 9, 75. [PubMed: 20920177]

44. Fei JY; Singh D; Zhang QC; Park S; Balasubramanian D; Golding I; Vanderpool CK; Ha T Determination of In Vivo Target Search Kinetics of Regulatory Noncoding RNA. Science 2015, 347 (6228), 1371–1374. [PubMed: 25792329]

45. Nevo-Dinur K; Nussbaum-Shochat A; Ben-Yehuda S; Amster-Choder O Translation-Independent Localization of mRNA in E. coli. Science 2011, 331 (6020), 1081–1084. [PubMed: 21350180]

46. Yuan P; Mao X; Chong KC; Fu J; Pan S; Wu S; Yu C; Yao SQ Simultaneous Imaging of Endogenous Survivin mRNA and On-Demand Drug Release in Live Cells by Using a Mesoporous Silica Nanoquencher. Small 2017, 13 (27), 1700569.

47. Prigodich AE; Seferos DS; Massich MD; Giljohann DA; Lane BC; Mirkin CA Nano-flares for mRNA Regulation and Detection. ACS Nano 2009, 2147–2152 [PubMed: 19702321]

48. Ren KW; Xu Y; Liu Y; Yang M; Ju HX A Responsive “Nano String Light” for Highly Efficient mRNA Imaging in Living Cells via Accelerated DNA Cascade Reaction. ACS Nano 2018, 12 (1), 263–271. [PubMed: 29253327]

49. Arora A; Sunbul M; Jaschke A Dual-colour Imaging of RNAs Using Quencher- and Fluorophore-binding Aptamers. Nucleic. Acids Res 2015, 43 (21), e144. [PubMed: 26175046]

50. Warner KD; Sjekloća L; Song WJ; Filonov GS; Jaffrey SR; Ferré-D’Amaré AR A Homodimer Interface without Base Pairs in an RNA Mimic of Red Fluorescent Protein. Nat. Chem. Biol 2017, 13, 1195–1201. [PubMed: 28945234]

51. Song WJ; Filonov GS; Kim H; Hirsch M; Li X; Moon JD,; Jaffrey SR Imaging RNA Polymerase III Transcription Using A Photostable RNA-fluorophore Complex. Nat. Chem. Biol 2017, 13, 1187–1194. [PubMed: 28945233]

52. Autour A; Jeng SCY; Cawte AD; Abdolahzadeh A; Galli A; Panchapakesan SSS; Rueda D; Ryckelynck M; Unrau PJ Fluorogenic RNA Mango Aptamers for Imaging Small Non-coding RNAs in Mammalian Cells. Nat. Commun 2018, 9 (1), 656. [PubMed: 29440634]

53. Surana S; Shenoy AR; Krishnan Y Designing DNA Nanodevices for Compatibility with the Immune System of Higher Organisms. Nat. Nanotechnol 2015, 10 (9), 741–747. [PubMed: 26329110]

54. Delebecque CJ; Lindner AB; Silver PA; Aldaye FA Organization of Intracellular Reactions with Rationally Designed RNA Assemblies. Science 2011, 333 (6041), 470–474. [PubMed: 21700839]

55. Sachdeva G; Garg A; Godding D; Way JC; Silver PA In Vivo Co-localization of Enzymes on RNA Scaffolds Increases Metabolic Production in A Geometrically Dependent Manner. Nucleic. Acids Res 2014, 42 (14), 9493–9503. [PubMed: 25034694]

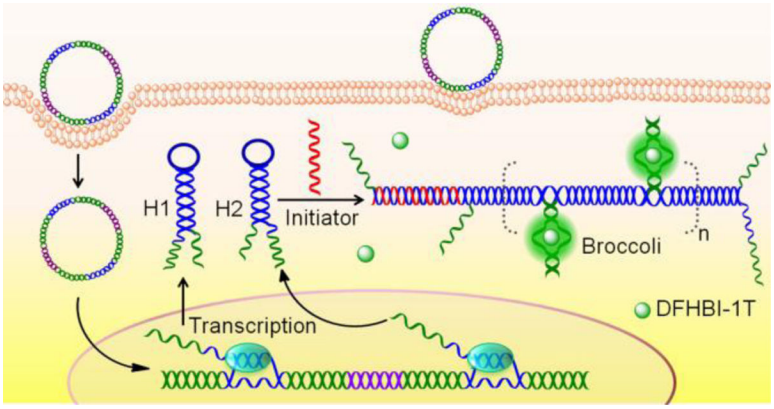

Figure 1.

Schematic of the genetically encoded INSIGHT system. After the cellular transcription of the H1 and H2 strands (blue) from a delivered vector, the binding of initiator RNA (red) triggers the cascaded H1/H2 hybridization. As a result, the reassembly of Broccoli (green) can be used for imaging the subcellular location of the initiator strand.

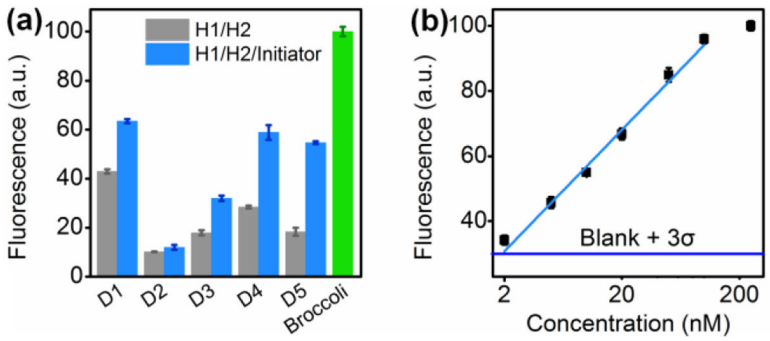

Figure 2.

Optimization and *in vitro* characterization of the INSIGHT system. (a) The fluorescence response of different sequence designs was measured after 4 h incubation in a solution containing 0 or 50 nM initiator RNA, 250 nM H1 and H2 (or Broccoli), and 5.0 μM DFHBI-1T. (b) Calibration curve for the initiator RNA detection. The horizontal line indicated the fluorescence intensity for estimating the limit of detection of the system. Shown are mean and SEM values of three independent replicates.

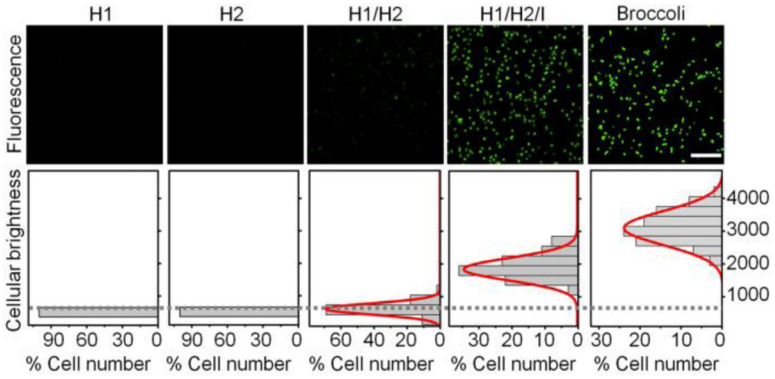

Figure 3.

Confocal fluorescence imaging of BL21 (DE3)* *E. coli* cells expressing, respectively, pETDuet-H1 (H1), pETDuet-H2 (H2), pETDuet-H1/H2 (H1/H2), pCDFDuet-initiator + pETDuet-H1/H2 (H1/H2/I), and pETDuet-Broccoli (Broccoli). Scale bar, 20 μm. Distribution of cellular fluorescence levels was measured from a total of 300 cells in each case. The dashed line indicated the averaged background signal as measured in cells expressing H1/H2.

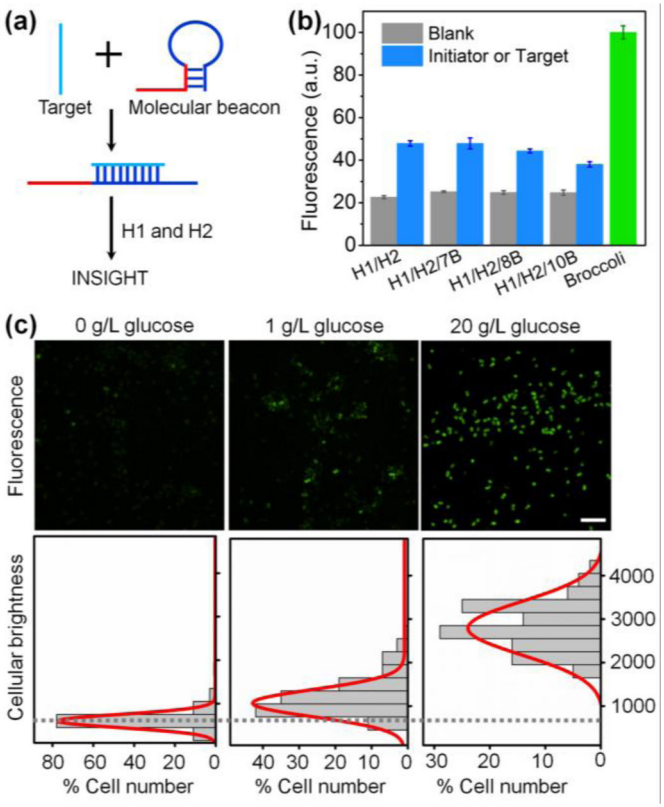

Figure 4.

A modular INSIGHT system for imaging SgrS. (a) Schematic of a general INSIGHT platform for target RNA detection. The target RNA hybridizes with the molecular beacon and releases an initiator strand (red) to trigger the hybridization chain reaction between H1 and H2. (b) Optimizing the number of stem base pairs in the molecular beacon. Fluorescence signal was measured after 4 h incubation in a solution containing 0 or 20 nM SgrS (or initiator for H1/H2), 250 nM H1 and H2 (or Broccoli), 250 nM molecular beacon, and 5.0 μM DFHBI-1T. Shown are mean and SEM values of three independent replicates. (c) Confocal fluorescence imaging of BL21 (DE3)* cells expressing pETDuet-H1/H2 and pCDFDuet-SgrSMB-7B (SgrS-targeting molecular beacon). Images were taken after 3 h incubation in the presence of 0, 1 g/L, or 20 g/L glucose. Scale bar, 10 μm. Distribution of cellular fluorescence levels was measured from a total of 300 cells in each case. The dashed line indicated the averaged background signal as measured in cells without glucose induction.

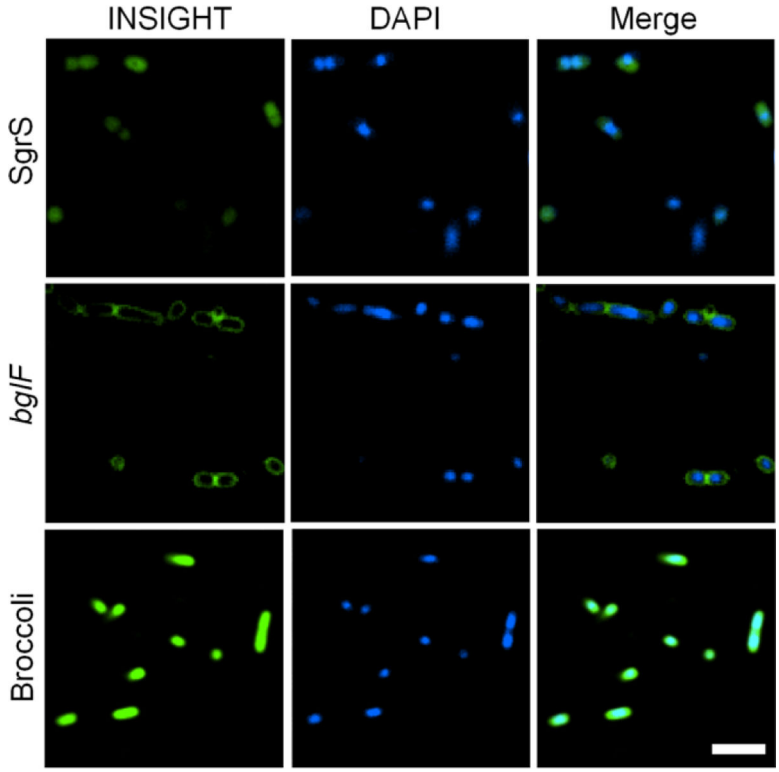

Figure 5.

Imaging the subcellular location of SgrS and *bglF* in BL21 (DE3)* cells. Confocal fluorescence imaging of cells expressing pETDuet-H1/H2 + pCDFDuet-SgrSMB-7B or pCDFDuet-*bglF*MB-7B (molecular beacon that targets SgrS or *bglF*), or pETDuet-Broccoli. DAPI was used to stain the nucleoid of *E. coli*. Scale bar, 5 μm.

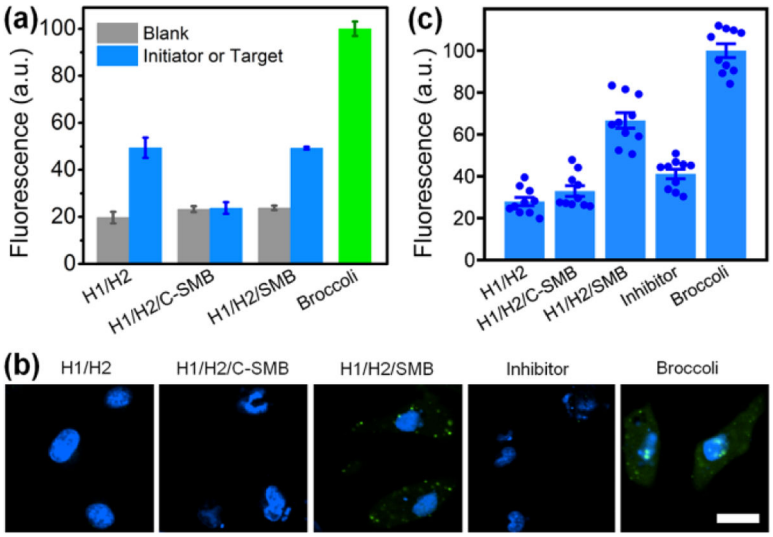

Figure 6.

(a) Fluorescence signals were measured in a solution containing 0 (blank) or 20 nM *survivin* RNA (or initiator), 250 nM H1 and H2 (or Broccoli), 250 nM molecular beacon, and 5.0 μM DFHBI-1T. Shown are mean and SEM from three replicated experiments. (b) Confocal fluorescence imaging in HeLa cells at 24 h after Lipofectamine® 3000-based transfection. Images were taken in the presence of 40 μM DFHBI-1T. 5 nM YM155 (inhibitor) was added to inhibit the generation of *survivin* mRNA. Scale bar, 10 μm. (c) Mean cellular fluorescence intensities in the experiments as shown in panel (b). Shown are mean and SEM from ten individual cells.